Journal of Solid State Chemistry **154,** 54–60 (2000)
doi:10.1006/jssc.2000.8811, available online at http://www.idealibrary.com on IDEAL®

Effect of Transition Metal Doping in YB_{66}[1]

Takaho Tanaka, Ying Shi,[2] Takao Mori, and Andreas Leithe-Jasper

National Institute for Research in Inorganic Materials, Namiki 1-1, Tsukuba, Ibaraki 305-0044, Japan

Received September 9, 1999; in revised form January 26, 2000; accepted January 30, 2000

The 3*d* (from Ti to Cu) and 4*d* (from Zr to Mo) transition metals were doped to YB_{66}. It was observed that the powder X-ray diffraction (XRD) intensities of their low-angle reflections like 200, 220, and 222 drastically changed from those of undoped YB_{66} without changing face-centered cubic symmetry, except for Co- and Ni-doped YB_{66}. On the other hand, the powder XRD patterns of Co- and Ni-doped YB_{66} showed new peaks assigned to the 210, 300, 410, and 421 reflections and so on, indicating that the crystal lattice of Co- and Ni-doped YB_{66} should be primitive. Single-crystal structure analysis of Cu-doped YB_{62} showed that basic boron icosahedral framework is unchanged from that of undoped YB_{66}. A new yttrium site at (0.25, 0.25, 0.25) and an interstitial Cu site at (0.144, 0.25, 0.25) were observed in addition to the original yttrium site at (0.0524, 0.25, 0.25). Single crystals of Cu-, Ni-, and Mo-doped YB_{66} were grown by the floating zone method using a xenon lamp image furnace. Specific heats of Cu- and Ni-doped YB_{66} were measured. A T linear contribution was observed in addition to the phonon T^3 term, suggesting that the amorphous-like phonon-related properties observed in undoped YB_{66} were retained in the transition metal-doped YB_{66}. © 2000 Academic Press

Key Words: **YB_{66}; transition metal doping; powder X-ray diffraction; electron diffraction; single-crystal growth; specific heat.**

INTRODUCTION

YB_{66} is a practical soft X-ray monochromator for dispersing synchrotron radiation in the energy range from 1 to 2 keV (1, 2). It is known to have a face-centered cubic crystal structure, space group *Fm*3*c*, and there are approximately 1584 boron atoms and 24 yttrium atoms per unit cell with a lattice constant of 23.44 Å. The boron framework of YB_{66} is basically made up of a 13-icosahedron unit $(B_{12})_{13}$, which is a so called "supericosahedron." Two kinds of supericosahedron that differ only by 90° rotation form two interpenetrating fcc lattices. Thus, there are 8 supericosahedra per unit cell, or 1248 icosahedra boron atoms in the unit cell. The remaining 336 atoms distribute on nonicosahedral cages, or B_{80} clusters, at the body center of each octant of the unit cell. The B_{80} cluster accommodates 42 boron atoms. The yttrium atoms statistically distribute over 48 sites which are equivalent to (0.0542, 0.25, 0.25) with 0.5 occupancy for YB_{66} (3, 4).

After the first installation of the YB_{66} soft X-ray monochromator on BL3-3 at Stanford Synchrotron Radiation Laboratory (late 1993) (5), its practical use is gradually spreading to soft X-ray beam lines at many synchrotron radiation (SR) facilities. Although YB_{66} satisfies all the X-ray and material property requirements for use as a soft X-ray monochromator in a synchrotron beam, particularly in the region 1–2 keV, the reflectivity of the 400 reflection ($2d = 11.76$ Å) which is of practical use is not high, so the output beam has an intensity of less than 10^{-3} of the incident beam under a double-crystal monochromator configuration. Because of the amorphous-like low thermal conductivity of YB_{66} (6) its use on brighter beam lines at third-generation SR facilities has not been practical yet. There is also a demand for a longer $2d$ value to disperse softer X rays down to about 0.5 keV because grating monochromators still have less resolution and reflectivity than crystal monochromators in this energy range.

A search for replaceable compounds in boron-rich borides could supply us with many new boron-rich borides like YB_{25} (7), YB_{50} (8), ScB_{19} (9), $ScB_{17}C_{0.25}$ (10), and $ScB_{15}C_{1.6}$ (11). However, except for YB_{50}, most of them decompose at high temperatures without melting, making it difficult to grow sizable and high quality crystals by the melt growth method. In the case of YB_{50}, the addition of a small amount of Si could change the melting behavior of YB_{50} and single crystals of $YB_{44}Si_{1.0}$ isostructural to YB_{50} could be grown by the floating zone method (12). However, it is quite difficult to improve crystal quality of this boron-rich yttrium borosilicide to the level required for monochromator grade and such high quality has not been achieved up to now.

Another idea to improve the monochromator characteristics of YB_{66} is to modify the crystal structure and reduce

[1] In this text, the notation of YB_{66} is conveniently used as the name of this compound which crystallizes in a significantly wide homogeneity range from YB_{56} to $YB_{\sim 70}$.

[2] Present address: Department of Chemical Engineering, Kansas State University, Manhattan, KS 66506.

0022-4596/00 $35.00

randomness in the crystal structure which includes about 50% site occupancy of yttrium ions and statistical distribution of only 42 boron atoms on a B_{80} cluster. Recently we found that transition metal doping in YB_{66} can modify strongly not only its X-ray diffraction characteristics but also the crystal structure itself. As seen in the review work (13), there are many investigations of the transition metal doping in β-rhombohedral boron, while up to now no one has reported such an investigation on YB_{66} as far as we know. This is the first report of transition metal doping in YB_{66}.

In the present investigation, powder X-ray diffraction (XRD) analyses were carried out on transition metal-doped YB_{66}. Single crystals of several of them were grown by the floating zone method. In addition, their low-temperature specific heats were measured to compare with that of undoped YB_{66}.

EXPERIMENTAL

Syntheses of transition metal-doped YB_{66} were carried out by the arc-melting method. First YB_n ($n = 56$ or 62) was synthesized by solid-state reaction between commercial YB_4 powder (3N, Sin-nihon Kinzoku Inc., Japan) and amorphous B powder (2N, SB-Boron Inc.) in a boron nitride crucible inserted in an inductively heated carbon-free composite susceptor at about 1700°C under vacuum for 1 h after both powders were thoroughly mixed and pressed into a pellet. Then the synthesized YB_n and a desired amount of transition metal were mixed and arc-melted. The arc-melting process was repeated two to three times, with the pellet being turned over to obtain better uniformity.

The pellet was crushed into a powder for XRD analysis using a silicon nitride mortar. The XRD measurements were carried out using a standard X-ray powder diffractometer (R-2000, Rigaku Co.) with Cu$K\alpha$ radiation by a graphite monochromator. The scanning step width is 0.02° and the sampling time is 1.2 s. per step. The $K\alpha_1$ peak intensities were determined after rejecting $K\alpha_2$ peaks, using RINT software (Rigaku Co.).

The electron diffraction patterns (EDPs) were derived at an acceleration voltage of 100 kV using a standard electron microscope (JEM-1010, JEOL).

For chemical analysis the pellet was crushed with a stainless-steel mortar; then the powder was washed with HCl solution and rinsed to remove stainless-steel contamination. After the powder was dissolved into $HNO_3 + HCl$ (1:1) solution, which was kept at 150°C for 16 h, yttrium, boron, and transition metal contents were determined by inductively coupled plasma atomic emission spectroscopy.

Single crystals of the transition metal-doped YB_{66} were grown by the floating zone (FZ) method using a xenon lamp single ellipsoidal mirror image furnace. Polycrystalline rods for a feed rod of FZ crystal growth were prepared by the arc-melting method or by the sintering method. The crystals were grown at the growth rate of 20 mm/h with counterrotation of both the feed rod and the growing crystal at about 40 rpm under a flowing Ar gas atmosphere.

Specific heat was measured by the transient heat pulse method (PPMS, Quantum Design Inc.) with a small temperature increase of $\sim 2\%$ relative to the system temperature. A rectangular sample was cut from a grown single crystal. A polished face of the sample was attached to an alumina plate holder using Apiezon N grease. Results from a blank run of the holder and grease were subtracted from the data to obtain the specific heat of the sample. The measured temperature region was 2 to 30 K.

RESULTS AND DISCUSSION

Powder XRD Analysis

The 3*d* (from Ti to Cu) and 4*d* (from Zr to Mo) transition metals were doped to YB_n ($n = 56$ or 62) using the arc-melting method. Crystals of YB_{56}, which is the yttrium richest composition in the homogeneity range of YB_{66}, are of the highest quality and are used as the practical soft X-ray monochromator (1, 2). On the other hand, crystals with the congruent composition of $n = 62$ can be grown without composition change during floating zone crystal growth. Because of these reasons both compositions of $n = 56$ and 62 were examined.

A change in the X-ray diffraction characteristics of YB_{66} by copper doping was found during the arc-melting experiment of carbon doping in YB_{66}. At first we expected that the change was caused by the carbon doping in YB_{66}, but later it was understood that the effect came from the copper doping. YB_{66} is a semiconducting material and has a rather high resistivity of about several hundred ohm-centimeter at room temperature. Because of this high resistivity, the arc discharge often does not couple directly to the YB_{66} specimen but instead to the water-cooled copper boat, which causes copper evaporation and successive incorporation into YB_{66}. We confirmed the effect of copper doping by the purposeful addition of copper powder to YB_{66}.

For other transition metals repetition of the arc melting was restricted to a minimum (two to three) to avoid codoping with copper and also evaporation loss during the arc-melting process. For these reasons the arc-melting experiments were performed only to determine the qualitative effect of transition metal doping. Actually the molar weight of the transition metals mixed before arc melting was the same as, that of yttrium in the YB_n specimen. In most cases it exceeded the maximum soluble content in YB_n and transition metal residue was observed. Weight loss after arc melting was not measured. Chemical analysis was made for only a few samples after removing the transition metal residue.

Notable lattice constant variation due to these dopings could not be observed. As two examples, the powder XRD patterns of Cu-doped YB_{62} and Mo-doped YB_{56} are shown in Fig. 1 and compared with that of the undoped one. It should be noted here that the XRD patterns of undoped YB_{62} and YB_{56} show little difference except for a small lattice constant increase for YB_{56} (23.460 Å) compared with YB_{62} (23.436 Å) (3). Chemical analysis of the doped samples showed the compositions to be $YB_{61.5}Cu_{1.0}$ and $YB_{56.0}Mo_{0.29}$, respectively. Among the striking features observed at low-angle reflections: (1) There was a drastic increase in the 200 reflection. This appeared most strongly in the Cu-doped case where the 200 reflection exceeds the 400 reflection; nevertheless the 200 reflection of the undoped sample is no more than 1/35th of the 400 reflection. For other transition metal-doped samples the 200 reflection became about half of the 400 reflection, as in the Mo-doped case shown in Fig. 1. (2) The 220 reflection was observed. (3) The 222 reflection disappeared. (4) There was an increase in the 420 reflection.

The increase in the 200 reflection ($2d = 23.5$ nm) suggests the possibility of developing a new crystal monochromator useful for dispersing X rays in the range 0.5 to 1 keV.

EDP analysis was carried out for the Cu-doped YB_{62} sample to determine whether the transition metal-doped YB_{66} maintains $Fm3c$ symmetry. Figure 2 shows the EDP of the [211] axis. The 311 reflection, which violates c-glide symmetry, can be clearly observed, suggesting that the space group of the Cu-doped YB_{62} is not $Fm3c$ but $Fm3$. This was confirmed later by a Weissenberg camera study where many hhl with odd h and l reflections could be observed. Surprisingly the 311 reflection could be observed even for the EDP

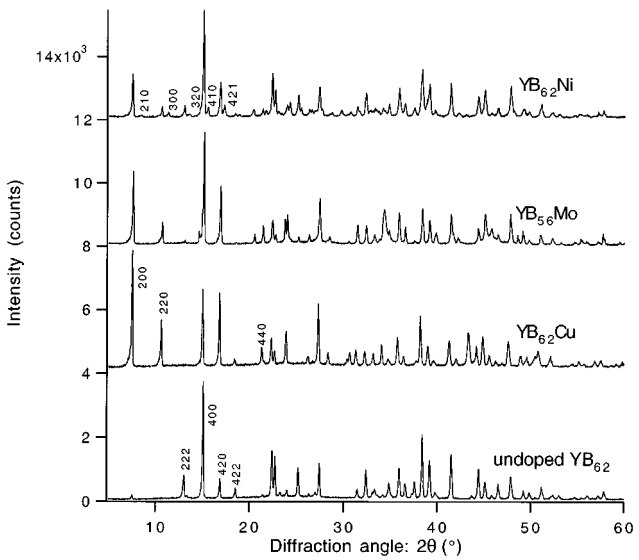

FIG. 1. Powder XRD patterns of Ni-doped YB_{56} (top), Mo-doped YB_{56} (second from top), Cu-doped YB_{62} (second from bottom), and undoped YB_{62} (bottom).

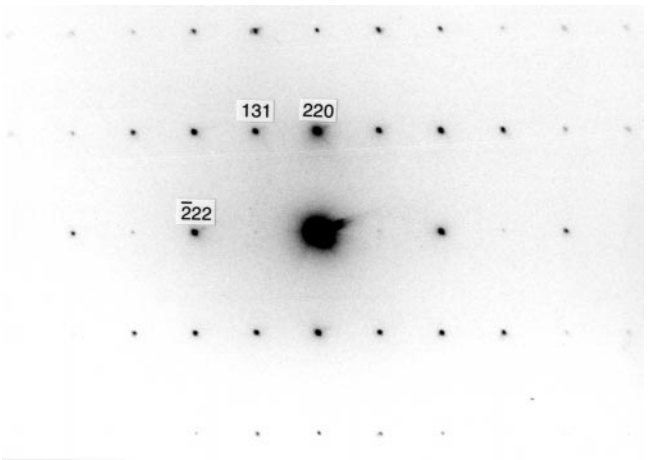

FIG. 2. Electron diffraction pattern along the [211] axis of Cu-doped YB_{62}.

of undoped YB_{62}, which suggests that the violation of c-glide symmetry is not due to the Cu doping effect but the original crystal structure of YB_{66} itself does not have c-glide symmetry. In fact, Richards and Kasper (3) have already reported that weak hhl reflections violating c-glide symmetry could be observed in their precession photograph even though they selected $Fm3c$ symmetry for simplicity. More detailed symmetry analysis of undoped YB_{66} should be undertaken.

Doping by the other transition metals can change the diffraction characteristics of YB_{66} in the same way as Cu or Mo doping without changing the face-centered cubic symmetry. However, the effect of Co or Ni doping manifests in a different way. As can be seen in Fig. 1, XRD analysis of $YB_{62}Ni_{0.3}$ shows the reflections of 210, 300, 320, 410, 421, and so on which violate the fcc extinction rule, indicating that Ni doping modified the fcc crystal structure of YB_{66} to a simple cubic one. Since this simple cubic structure of Ni-doped YB_{66} can be understood to be a new structure, the indexing result is listed in Table 1. No extinction could be found from the indexing result. The lattice constant 23.446(8) Å of this $YB_{62}Ni_{0.3}$ showed little difference from that of pure YB_{62} (23.4364(6) Å) (4) as mentioned in the first part of this section. Co doping also has the same effect on YB_{66} crystal structure.

Single-Crystal Structure Analysis

To understand why transition metal doping in YB_{66} can have such a large effect on diffraction characteristics, single-crystal structure analysis of Cu-doped YB_{62} was done using a four-circle diffractometer. The single-crystal sample was selected from the fragments obtained by cracking the arc-melted sample whose starting composition was $YB_{62}Cu_{1.0}$ and XRD pattern was similar to that shown in Fig. 1. Here,

TABLE 1
Powder X-Ray Diffraction Data of $YB_{62}NI_{0.3}$

h	k	l	D_{calc}	D_{obs}	I/I_o	h	k	l	D_{calc}	D_{obs}	I/I_o
2	0	0	11.7231	11.7464	23	8	4	4	2.3930	2.3927	10
2	1	0	10.4855	10.5177	4	10	0	0	2.3446	2.3446	46
2	2	0	8.2895	8.2924	8	10	1	0	2.3330	2.3329	11
3	0	0	7.8154	7.8242	7	10	2	0	2.2991	2.2986	42
2	2	2	6.7684	6.7735	11	9	5	1	2.2666	2.2674	9
3	2	0	6.5028	6.5057	5	10	4	0	2.1769	2.1782	25
4	0	0	5.8616	5.8626	100	10	4	2	2.1403	2.1407	7
4	1	0	5.8666	5.6831	13	11	0	0	2.1315	2.1311	6
4	2	0	5.2427	5.2421	32	10	5	0	2.0971	2.0962	5
4	2	1	5.1164	5.1159	16	8	8	2	2.0407	2.0404	27
4	2	2	4.7859	4.7921	4	9	6	4	2.0331	2.0317	7
5	0	0	4.6893	4.6916	5	10	6	0	2.0105	2.0104	25
5	2	0	4.3539	4.3541	9	10	6	2	1.9816	1.9820	6
4	4	0	4.1448	4.1450	10	12	0	0	1.9539	1.9546	11
4	4	1	4.0185	4.0810	9	10	7	0	1.9208	1.9202	5
5	3	1	3.9631	3.9623	39	12	2	2	1.9017	1.9028	32
4	4	2	3.9077	3.9073	20	12	4	0	1.8536	1.8540	9
6	1	0	3.8545	3.8604	7	10	8	0	1.8308	1.8309	9
6	1	1	3.8035	3.8082	6	10	6	6	1.7878	1.7873	12
6	2	0	3.7072	3.7080	11	13	3	1	1.7525	1.7516	6
5	4	0	3.6617	3.6628	16	12	6	0	1.7476	1.7472	6
6	2	2	3.5347	3.5367	21	12	6	2	1.7285	1.7288	5
6	3	0	3.4952	3.4957	11	11	8	2	1.7055	1.7055	4
4	4	4	3.3842	3.3859	11	13	5	1	1.6790	1.6795	4
7	0	0	3.3495	3.3484	10	10	10	0	1.6579	1.6577	5
6	4	0	3.2514	3.2524	30	10	10	2	1.6416	1.6419	6
6	4	1	3.2206	3.2202	10	12	8	2	1.6103	1.6097	7
7	2	2	3.1055	3.1038	8	14	4	2	1.5953	1.5949	7
6	5	0	3.0020	3.0036	9	10	10	6	1.5262	1.5263	8
7	4	0	2.9082	2.9081	8	12	10	0	1.5010	1.5013	6
8	2	0	2.8433	2.8431	12	12	10	2	1.4888	1.4887	4
8	2	1	2.8226	2.8239	7	13	9	1	1.4799	1.4798	4
6	6	0	2.7632	2.7643	22	14	8	0	1.4541	1.4544	10
8	3	0	2.7442	2.7413	6	14	6	6	1.4322	1.4321	8
5	5	5	2.7073	2.7074	8	12	10	6	1.4012	1.4012	5
6	6	2	2.6895	2.6900	11	13	11	1	1.3744	1.3747	5
8	3	2	2.6720	2.6697	11	17	3	1	1.3559	1.3559	12
8	4	0	2.6214	2.6212	14	12	12	4	1.3447	1.3443	5
9	0	0	2.6051	2.6049	9	18	0	0	1.3026	1.3030	7
9	1	1	2.5736	2.5716	15	18	2	2	1.2868	1.2865	11
6	6	4	2.4994	2.4981	38	14	12	2	1.2641	1.2639	5
9	2	2	2.4853	2.4861	12	18	4	4	1.2427	1.2429	8
9	3	1	2.4578	2.4558	19	18	6	0	1.2357	1.2355	3
						16	10	4	1.2156	1.2159	5

only the preliminary results are given in brief; detailed structure analysis will be the subject of another paper.

The results showed that the boron icosahedral framework of Cu-doped YB_{62} remained the same as that of undoped YB_{66} and that a new yttrium site appeared at the body center of the octant of the unit cell, i.e., (0.25, 0.25, 0.25), where the B_{80} cluster is also located. Occupancies of some boron sites in the B_{80} cluster become nearly zero to create the new Y site. An interstitial Cu site is found at (0.144, 0.25, 0.25), which is just between the new Y site and the original Y site (0.0524, 0.25, 0.25). The original Y site is slightly pushed toward the face center of the octant from its beginning position (0.0563, 0.25, 0.25) in undoped YB_{62}. A ratio of the structure factors $F(200)/F(400)$ of Cu-doped YB_{62} increased to 0.57 from 0.046 for undoped YB_{66}. Since the dominant difference between the crystal structures of Cu-doped YB_{62} and undoped YB_{66} is the appearance of the new Y site and the interstitial Cu site and there is little difference in the boron lattices, these metal sites must contribute largely to the intensity of the 200 reflection.

Single-Crystal Growth

To develop soft X-ray monochromators a sizable single crystal is indispensable. Single crystals of Cu-, Ni-, or Mo doped YB_{62} or YB_{56} were grown by the floating zone method.

During the floating zone process using a sintered feed rod, one part of the feed rod would start melting incongruently as the molten zone approached that part. The observed melt which includes most of the doped Cu or Ni in that part has a strong tendency to move away from the molten zone through open pores in the feed rod, preventing dissolution of Cu or Ni into the molten zone. As a result the crystal obtained was not doped with Cu or Ni. Probably this is due to the fact that both Cu and Ni have rather low melting temperatures compared with YB_{66}. Thus, for Cu- or Ni-doped samples, dense and pore-free polycrystalline feed rods were necessary for preparation by the arc-melting method.

A YB_{62} sintered rod and Cu granular particles with a composition of $YB_{62}Cu_{1.0}$ were arc-melted several times to make them into a 6-mm-diameter thin rod. During the floating zone pass violent Cu evaporation was observed, which reduced the Cu content of the crystal. The crystal obtained is shown in Fig. 3. Powder XRD analysis of the crystal showed that the intensity of the 200 reflection was only about one-seventh that of the 400 reflection. The ratio is much smaller than that of the arc-melted sample shown in Fig. 1. To achieve high crystallographic quality of the crystal for monochromator use at least a double zone pass is necessary (1), but Cu cannot be expected to remain in the crystal after the double zone pass. Elements less volatile than Cu should be selected as dopant.

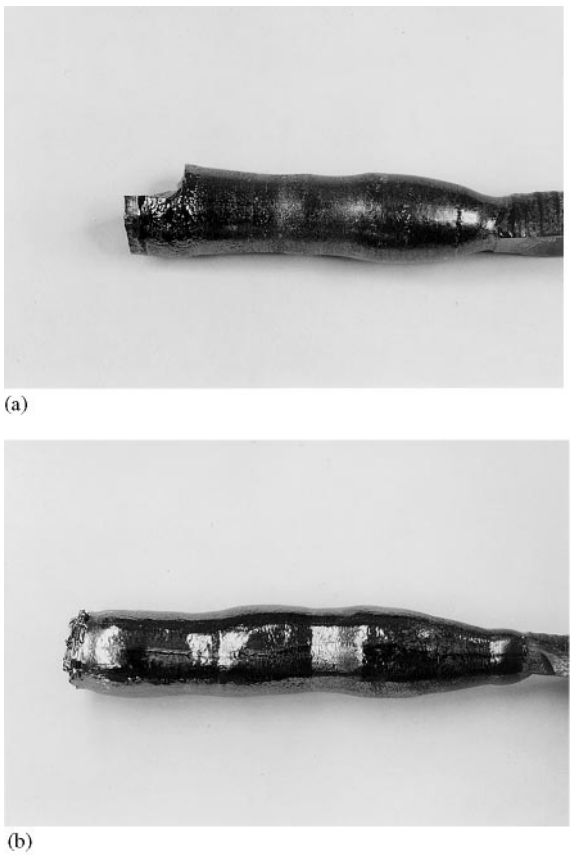

FIG. 3. Single crystals of Cu-doped YB_{62} (top) and Ni-doped YB_{62} (bottom) grown by the floating zone method.

A floating zone pass trial for a $YB_{62}Ni_{1.0}$ rod prepared by the arc-melting method failed rather quickly because of molten zone instability seemingly due to Ni accumulation in the molten zone, which suggested that the maximum Ni content is less than $YB_{62}Ni_{1.0}$. Another zone pass trial for a $YB_{62}Ni_{0.2}$ rod was also not as straightforward, but at least a single crystal was obtained as shown in Fig. 3. The powder XRD intensity of the 200 reflection was also about one-seventh that of the 400 reflection. Further investigation is necessary to achieve the maximum Ni doping effect observed for the arc-melted sample.

The feed rods prepared by the arc-melting method have an irregular shape, however, and lack uniformity of Cu or Ni distribution in the rods, which made a stable zone pass quite difficult. It seemed almost hopeless to grow high-quality single crystals doped with Cu or Ni. If transition metals that are less volatile and form high-melting-temperature borides are selected, a stable zone pass may be expected by using feed rods prepared by the sintering method.

Following the above idea Mo was selected as a dopant. Mo-doped crystals could be grown by simply using a sintered polycrystalline rod. Compositions of the feed rod and of the initial molten zone were adjusted to be $YB_{56}Mo_{0.6}$ and $YB_{40}Mo_{1.8}$, respectively, expecting the equilibrium relation between yttrium and boron at the growth interface to be the same as that of undoped YB_{56} and the Mo partition coefficient to be about 0.3. The zone pass was rather stable initially but gradually the melting temperature of the molten zone seemed to decrease. Finally the molten zone became unstable and the zone pass could not be continued. Compositions of the crystal parts at the seed end, middle, and zone end were $YB_{56.5}Mo_{0.26}$, $YB_{56.0}Mo_{0.29}$, and $YB_{47.5}Mo_{0.6}$, respectively. The zone end crystal included a small amount of YB_{12} phase. We can estimate the partition coefficient of Mo to be about 0.15, which is half of the expected value. The Mo contents of the seed end and the middle part crystals are lower than that of the feed rod, causing an increase in Mo content in the molten zone and a corresponding decrease in the melting temperature. The powder XRD intensity of the 200 reflection at the middle part was about a half that of the 400 reflection, which almost realized the maximum doping effect achieved by the arc-melting method (shown in Fig. 1). Thus, Mo is a more promising element than Cu or Ni.

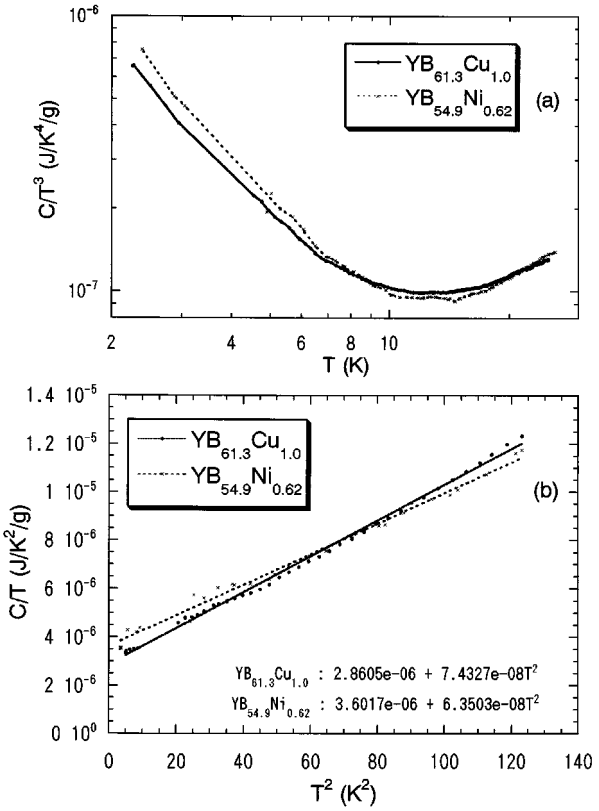

FIG. 4. Specific heats of Cu-doped YB_{62} and Ni-doped YB_{56}. (a) $C/T3$-versus-T plot and (b) C/T-versus-T^2 plot.

Specific Heat Measurement

Results of the specific heat measurements of $YB_{61.3}Cu_{1.0}$ and $YB_{54.9}Ni_{0.62}$ are shown in Fig. 4. The qualitative behavior of the specific heat is similar to that obtained for undoped YB_{66} (14). At lower temperature the T^3 dependence usually observed for Debye solids such as β-boron (15) is not observed. Following Ref. 13, if specific heat divided by T^3 is plotted, a rapid rise below 12 K is observed as shown in Fig. 4a. This indicates a contribution to the specific heat in addition to the phonon T^3 term. The data below 12 K can be fit by the equation

$$C = c_1 T + c_2 T_3. \qquad [1]$$

$c_1 = 29$ erg/g/K^2 and $c_2 = 0.74$ erg/g/K^4 for the Cu-doped sample and $c_1 = 36$ erg/g/K^2 and $c_2 = 0.65$ erg/g/K^4 for the Ni-doped sample are determined. If the results are compared with that of YB_{66}, $c_1 = 23$ erg/g/K^2 and $c_2 = 0.89$ erg/g/K^2 (14), a tendency for the linear terms to become larger while the coefficient of the T^3 term becomes smaller is observed. In the case of metals the T linear term has been attributed to the electronic specific heat. However, since YB_{66} is a semiconductor having high resistivity as mentioned before and glass-like thermal conductivity, the T linear term of YB_{66} has been attributed not to the electronic specific heat but to the amorphous-like lattice behavior (14). Since the general magnitudes of the T linear term are the same for undoped YB_{66} and the sample measured in this work, the T linear contribution to the specific heat can probably be attributed to the same amorphous-like behavior of Cu- or Ni-doped YB_{66}, which suggests that the phonon-related property of the doped YB_{66} is basically unchanged even though some structure modifications occurred with doping.

CONCLUSION

The 3*d* (from Ti to Cu) and 4*d* (from Zr to Mo) transition metals were doped to YB_{66}. Powder XRD patterns of transition metal-doped YB_{66}, except Co- and Ni-doped YB_{66}, showed large differences from that of undoped YB_{66}; i.e., the 200 reflection, which is very weak for undoped YB_{66}, became so strong as to be comparable to the 400 reflection, the 220 reflection appeared, the 222 reflection nearly disappeared, and so on. In the EDP of Cu-doped YB_{66} the 311 reflection, which violates *c*-glide symmetry, could be observed, suggesting that the space group of Cu-doped YB_{66} is not *Fm*3*c* but *Fm*3. Single-crystal structure analysis of Cu-doped YB_{66} showed that the basic boron icosahedral framework of doped YB_{66} is unchanged from that of undoped YB_{66}, but not only Cu at the interstitial site but also occupation of yttrium ions at a new site of (0.25, 0.25, 0.25) was observed. On the other hand, powder XRD patterns of Co- and Ni-doped YB_{66} showed new peaks which could be assigned to the 210, 300, 410, and 421 reflections and so on, violating the extinction rule of fcc lattice, indicating that the crystal lattices of Co- and Ni-doped YB_{66} should be primitive.

Single crystals of Cu-, Ni-, and Mo-doped YB_{66} were grown by the floating zone method using the xenon lamp image furnace. To grow high-crystallographic-quality single crystals for monochromator use selection of the most suitable element is necessary.

Specific heats of Cu- and Ni-doped YB_{66} were measured. The specific heat divided by T^3 showed a rapid rise below 12 K, which is due to a T linear contribution in addition to the phonon T^3 term. This temperature dependence is similar to that of undoped YB^{66}, suggesting that the doped YB_{66} retained the amorphous-like phonon related properties.

ACKNOWLEDGMENTS

The authors are indebted to Mr. S. Takenouchi and Mr. Y. Kitami of NIRIM for chemical analysis and electron diffractometry, respectively.

REFERENCES

1. T. Tanaka, Z. U. Rek, J. Wong, and M. Rowen, *J. Cryst. Growth* **192,** 141 (1998).
2. J. Wong, T. Tanaka, M. Rowen, F. Schäfers, B. R. Müler, and Z. U. Rek, *J. Synch. Radiat.* **6,** 1086 (1999).
3. S. M. Richards and J. S. Kasper, *Acta Crystallogr. Sect. B* **25,** 237 (1969).
4. I. Higashi, K. Kobayashi, T. Tanaka, and Y. Ishizawa, *J. Solid State Chem.* **133,** 16 (1997).
5. M. Rowen, Z. U. Rek, Joe Wong, T. Tanaka, G. N. George, I. J. Pickering, G. H. Via, and G. E. Brown, Jr., *Syn. Rad. News* **6**(3), 25 (1993).
6. P. A. Medwick, R. O. Pohl, and T. Tanaka, *Jpn. J. Appl. Phys. Ser.* **10,** 106 (1994).
7. T. Tanaka, S. Okada, Y. Yu, and Y. Ishizawa, *J. Solid State Chem.* **133,** 122 (1997).
8. T. Tanaka, S. Okada, and Y. Ishizawa, *J. Alloys Compd.* **205,** 281 (1994).
9. T. Tanaka, S. Okada, and V. N. Gurin, *J. Alloys Compd.* **267,** 211 (1998).
10. T. Tanaka, *J. Alloys Compd.* **270,** 132 (1998).
11. Y. Shi, A. Leithe-Jasper, T. Tanaka, *J. Solid State Chem.* accepted.
12. T. Tanaka, S. Okada, and Y. Ishizawa, *J. Solid State Chem.* **133,** 55 (1997).
13. T. Lundström, *AIP Conf. Proc.* **140,** 19 (1989).
14. D. G. Cahill, H. E. Fischer, S. K. Watson, R. O. Pohl, and G. A. Slack, *Phys. Rev. B* **40,** 3254 (1989).
15. P. R. H. Turkes, E. T. Shwartz, and R. O. Pohl, *AIP Conf. Proc.* **140,** 346 (1989).